Inorganic Chemistry
Article

Inorg. Chem. **2010**, *49*, 10427–10435 **10427**
DOI: 10.1021/ic1012999

Synthesis, Structure, and Solution Properties of $[(\text{mim-TASN})FeCl_2]^+$ and Its μ-Oxo Derivative

Jinlan Cui, Mark S. Mashuta, Robert M. Buchanan, and Craig A. Grapperhaus*

Department of Chemistry, University of Louisville, Louisville, Kentucky 40292, United States

Received June 29, 2010

A series of iron(III) complexes based on the tetradentate ligand 4-((1-methyl-1*H*-imidazol-2-yl)methyl)-1-thia-4,7-diazacyclononane (L) has been synthesized, and their solution properties investigated. Addition of $FeCl_3$ to methanol solutions of L yields $[LFeCl_2]FeCl_4$ as a dark red solid. X-ray crystallographic analysis reveals a pseudo-octahedral environment around iron(III) with the three nitrogen donors of L coordinated facially. Ion exchange reactions with $NaPF_6$ in methanol facilitate chloride exchange resulting in a different diastereomer for the $[LFeCl_2]^+$ cation. X-ray analysis of $[LFeCl_2]PF_6$ finds meridional coordination of the three nitrogen donors of L. Electrochemical studies of $[LFeCl_2]^+$ in acetonitrile display a single Fe(III)/(II) reduction potential at -280 mV versus ferrocenium/ferrocene. In methanol, a broad cathodic wave is observed because of partial exchange of one chloride for methoxide with half-potentials of -170 mV and -440 mV for $[LFeCl_2]^{+/0}$ and $[LFeCl(OCH_3)]^{+/0}$, respectively. The equilibrium constants for chloride exchange are 7×10^{-4} M^{-1} for Fe(III) and 2×10^{-8} M^{-1} for Fe(II). In aqueous solutions chloride exchange yields three accessible complexes as a function of pH. Strongly acidic conditions yield the aqua complex $[LFeCl(OH_2)]^{2+}$ with a measured pK_a of 3.8 $\pm$ 0.1. Under mildly acidic conditions, the μ-OH complex $[(LFeCl)_2(OH)]^{3+}$ with a pK_a of 6.1 $\pm$ 0.3 is obtained. The μ-oxo complex $[(LFeCl)_2(O)]^{2+}$ is favored under basic conditions. The diiron Fe(III)/Fe(III) complexes $[(LFeCl)_2(OH)]^{3+}$ and $[(LFeCl)_2(O)]^{2+}$ can be reduced by one electron to the mixed valence Fe(III)/Fe(II) derivatives at -170 mV and -390 mV, respectively. From pH dependent voltammetric studies, the pK_a of the mixed valent μ-OH complex $[(LFeCl)_2(OH)]^{2+}$ is calculated at 10.3.

Introduction

Nature provides several mononuclear non-heme iron enzymes that catalyze a variety of essential physiological reactions including oxidations and hydrolysis.[1−6] The mechanism of activation involves coordination and transport of O_2, water, or other substrates at the metal center via a variable coordination site. It is known that small molecule non-heme complexes containing dissociable ligands can be exploited as potential functional active site mimics. Most studies involving these model complexes, however, are performed in non-aqueous solvents that are also non-protic[5,7] which is in stark contrast to the aqueous environment present at the active sites of metalloenzymes. While some studies have investigated non-heme complexes under aqueous conditions,[8−11] there is a surprising paucity that utilize only a single complex under various solvent conditions. To address this we are currently evaluating the effect of solvent on ligand exchange, as well as, the influence of other donor atoms on ligand lability.

Under aqueous conditions, non-heme complexes with labile ligands are well-known to yield μ-oxo diiron complexes in the presence of base.[12] This is attributed to the strong Lewis acidity of the metal that significantly lowers the pK_a of water upon coordination. The μ-oxo derivative represents a conjugate base of the water-bound complex and the acid/base

*To whom correspondence should be addressed. E-mail: grapperhaus@louisville.edu.

(1) Bruijnincx, P. C. A.; van Koten, G.; Gebbink, R. *Chem. Soc. Rev.* **2008**, *37*, 2716–2744.
(2) Bugg, T. D. H.; Ramaswamy, S. *Curr. Opin. Chem. Biol.* **2008**, *12*, 134–140.
(3) Kovaleva, E. G.; Lipscomb, J. D. *Nat. Chem. Biol.* **2008**, *4*, 186–193.
(4) Abu-Omar, M. M.; Loaiza, A.; Hontzeas, N. *Chem. Rev.* **2005**, *105*, 2227–2252.
(5) Kovacs, J. A. *Chem. Rev.* **2004**, *104*, 825–848.
(6) Solomon, E. I.; Brunold, T. C.; Davis, M. I.; Kemsley, J. N.; Lee, S. K.; Lehnert, N.; Neese, F.; Skulan, A. J.; Yang, Y. S.; Zhou, J. *Chem. Rev.* **2000**, *100*, 235–349.
(7) Costas, M.; Mehn, M. P.; Jensen, M. P.; Que, L. *Chem. Rev.* **2004**, *104*, 939–986.
(8) Malkhasian, A. Y. S.; Finch, M. E.; Pawlak, P. L.; Anderson, J. M.; Brennessel, W. W.; Chavez, F. A. *Z. Anorg. Allg. Chem.* **2008**, *634*, 1087–1092.
(9) Verge, F.; Lebrun, C.; Fontecave, M.; Ménage, S. *Inorg. Chem.* **2002**, *42*, 499–507.
(10) Duboc-Toia, C.; Menage, S.; Vincent, J.-M.; Averbuch-Pouchot, M. T.; Fontecave, M. *Inorg. Chem.* **1997**, *36*, 6148–6149.
(11) Neimann, K.; Neumann, R.; Rabion, A.; Buchanan, R. M.; Fish, R. H. *Inorg. Chem.* **1999**, *38*, 3575–3580.
(12) Kurtz, D. M. *Chem. Rev.* **1990**, *90*, 585–606.

Published on Web 10/14/2010

Scheme 1. Synthetic Pathways

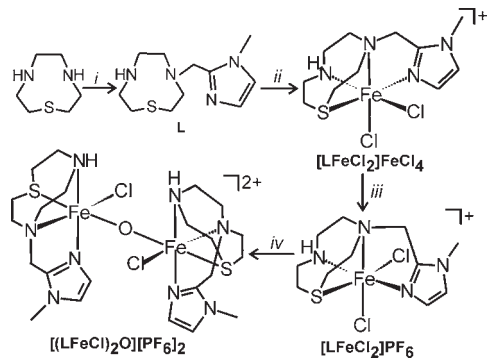

equilibrium is a fundamental component of the aqueous solution chemistry of mononuclear non-heme complexes, eq 1.

$$2\mathrm{LFe{-}OH_2}^{n+} + 2\mathrm{H_2O} \rightleftarrows \mathrm{LFe{-}O{-}FeL}^{(n-2)+} + 2\mathrm{H_3O}^{+} \quad (1)$$

Further, the μ-oxo complexes mimic dinuclear non-heme enzymes, such as methane monooxygenase, ribonucleotide reductase, and purple acid phosphatase.[6,13] Numerous studies of the redox chemistry of μ-oxo diiron complexes have been reported. Phenanthroline based complexes undergo a single, 2 electron reduction of the $Fe^{III}-O-Fe^{III}$ core to $Fe^{II}-O-Fe^{II}$ resulting in dissociation to mononuclear counterparts.[14−17] Most other complexes undergo one electron reduction of the $Fe^{III}-O-Fe^{III}$ to a mixed valent $Fe^{III}-O-Fe^{II}$ species; the stability of which is ligand dependent.[18−27]

In the current manuscript, we report the synthesis and characterization of the tetradentate ligand 4-((1-methyl-1*H*-imidazol-2-yl)methyl)-1-thia-4,7-diazacyclononane (L) and its iron derivatives, Scheme 1. The solution properties of $[LFeCl_2]^+$ have been investigated by spectroscopic and electrochemical techniques in both non-protic (acetonitrile) and protic (methanol and water) conditions. The results reveal two distinct chloride donors in the $[LFeCl_2]^+$ unit. One chloride remains coordinated in solution, while the other is substitutionally labile leading to a series of solution equilibria as a function of solvent, oxidation state, and pH.

Experimental Section

Materials and Methods. All reagents were obtained from commercially available sources and used as received unless otherwise noted. Solvents were dried and freshly distilled using standard techniques under a nitrogen atmosphere. Reactions were conducted using standard Schlenk techniques under an argon atmosphere or in an argon-filled glovebox unless otherwise noted. 1-Methyl-1*H*-imidazole-2-carboxaldehyde was prepared according to published methods.[28] 1-Thia-4,7-diazacyclononane (TASN) was prepared following the method described by Mattes et al.,[29] which is an adapation of earlier methods of Gahan et al.[30] and Hancock et al.[31]

4-((1-Methyl-1*H*-imidazol-2-yl)methyl)-1-thia-4,7-diazacyclononane (L). TASN (3.00 g, 20.5 mmol) was combined with 1-methyl-1*H*-imidazole-2-carboxaldehyde (3.15 g, 28.6 mmol) in 340 mL of dry methanol under Argon. The mixture was refluxed for 30 min and cooled to 0 °C using an ice bath. Sodium borohydride (3.49 g, 92.2 mmol) was added, and the reaction mixture was stirred for an additional 2 h. Unreacted $NaBH_4$ was quenched with 5 N HCl. The pH of solution was adjusted to 7, and the resulting sodium borate salt was removed by filtration. The filtrate was taken to dryness under reduced pressure leaving a yellow oil. The oil was dissolved in a minimum amount of water made alkaline by Na_2CO_3 (pH of solution was adjusted to 10) and extracted with 3 × 50 mL portions of the chloroform. The combined extracts were dried over sodium sulfate, and chloroform was removed under reduced pressure to give a crude product as a yellow oil. The compound was purified by Al_2O_3 column chromatography using ethyl acetate to remove impurities followed by methanol as eluant to obtain the ligand (L) as a brown oil. Yield: 3.83 g (15.9 mmol, 77.7%). ^{1}H NMR (δ, ppm, $CDCl_3$) 6.96 (d, 1H, C*H* of imidazole ring), 6.82 (d, 1H, C*H* of imidazole ring), 3.84 (s, 2H, CH_2), 3.57 (s, 3H, CH_3), 3.55 (t, 2H, $HNCH_2CH_2N$), 3.35 (t, 2H, $HNCH_2CH_2S$), 3.14 (t, 2H, $HNCH_2CH_2S$), 3.09 (t, 2H, SCH_2CH_2N), 2.85 (t, 2H, $HNCH_2CH_2N$), 2.54 (t, 2H, SCH_2CH_2N). ^{13}C{^{1}H}NMR (δ, ppm, $CDCl_3$), 145.19 (s, TASN−CH_2-*C*-imidazole), 126.91 (s, *C*H of imidazole ring), 121.54 (s, *C*H of imidazole ring, close to $N(CH_3)$), 58.20 (s, SCH_2CH_2N), 51.91 (s, $HNCH_2CH_2N$), 51.09 (s, CH_2), 48.81 (s, $HNCH_2CH_2S$), 46.40 (s, $HNCH_2CH_2N$), 34.11 (s, SCH_2CH_2N), 32.43 (s, CH_3), 30.09 (s, $HNCH_2CH_2S$).

[LFeCl$_2$]FeCl$_4$. To a solution of 1.69 g (10.4 mmol) of $FeCl_3$ in 4 mL of dry methanol was added via cannula a solution of 0.99 g (4.1 mmol) of ligand (**L**) in 8 mL of methanol. After the mixture was heated to reflux for 1 h, a dark red precipitate formed. The dark red solid was isolated by filtration and washed with dry diethyl ether and vacuum-dried. Yield: 1.45 g (2.57 mmol, 62.4%). X-ray quality crystals were obtained by slow evaporation of dichloromethane solution of **1** at room temperature. IR (KBr pellet) cm^{-1}: 3427 (br), 3225 (s), 3156 (m), 3136 (m), 1498 (s), 1455 (s), 1419 (m), 1404 (m), 1162 (s), 1096 (m), 1067 (s), 997 (m), 944 (m), 798 (m), 750 (s), 656 (m), 463 (m). (+)ESI-MS, *m*/*z* calcd. for $[C_{11}H_{20}N_4SFeCl_2]^+$, $[LFeCl_2]^+$ 366.01; Found, 366.00; $[LFeCl(OCH_3)]^+$ 362.06; Found, 362.06; $[(LFeCl(OH)]^+$ 348.04; Found, 348.03, $[L^{-H}FeCl]^+$ 330.04; Found, 330.03. Elem. anal. Calcd. for $C_{11}H_{20}N_4SFe_2Cl_6$: C, 23.39; H, 3.57; N, 9.92. Found: C, 23.38; H, 3.50; N, 9.88.

(13) Mitic, N.; Smith, S. J.; Neves, A.; Guddat, L. W.; Gahan, L. R.; Schenk, G. *Chem. Rev.* **2006**, *106*, 3338–3363.
(14) Wang, Q. X.; Jiao, K.; Sun, W.; Jian, F. F.; Hu, X. *Eur. J. Inorg. Chem.* **2006**, 1838–1845.
(15) Dunand-Sauthier, M. N. C.; Deronzier, A.; Toia, C. D.; Fontecave, M.; Gorgy, K.; Lepretre, J. C.; Menage, S. *J. Electroanal. Chem.* **1999**, *469*, 53–62.
(16) Walczak, M. M.; Flynn, N. T. *J. Electroanal. Chem.* **1998**, *441*, 43–49.
(17) Chen, S. M. *Inorg. Chim. Acta* **1996**, *249*, 143–150.
(18) Parrilha, G. L.; Ferreira, S. S.; Fernandes, C.; Silva, G. C.; Carvalho, N. M. F.; Antunes, O. A. C.; Drago, V.; Bortoluzzi, A. J.; Horn, A. *J. Braz. Chem. Soc.* **2010**, *21*, 603–613.
(19) Grohmann, A. *Dalton Trans.* **2010**, *39*, 1432–1440.
(20) Shakya, R.; Powell, D. R.; Houser, R. P. *Eur. J. Inorg. Chem.* **2009**, 5319–5327.
(21) Do, L. H.; Lippard, S. J. *Inorg. Chem.* **2009**, *48*, 10708–10719.
(22) López, J. P.; Heinemann, F. W.; Grohmann, A.; Horner, O.; Latour, J.-M.; Ramachandraiah, G. *Inorg. Chem. Commun.* **2004**, *7*, 773–776.
(23) Mukherjee, J.; Balamurugan, V.; Gupta, R.; Mukherjee, R. *Dalton Trans.* **2003**, 3686–3692.
(24) Musie, G.; Lai, C. H.; Reibenspies, J. H.; Sumner, L. W.; Darensbourg, M. Y. *Inorg. Chem.* **1998**, *37*, 4086–4093.
(25) Nivorozhkin, A. L.; AnxolabehereMallart, E.; Mialane, P.; Davydov, R.; Guilhem, J.; Cesario, M.; Audiere, J. P.; Girerd, J. J.; Styring, S.; Schussler, L.; Seris, J. L. *Inorg. Chem.* **1997**, *36*, 846–853.
(26) Holz, R. C.; Elgren, T. E.; Pearce, L. L.; Zhang, J. H.; O′Connor, C. J.; Que, L. *Inorg. Chem.* **1993**, *32*, 5844–5850.
(27) Hartman, J. A. R.; Rardin, R. L.; Chaudhuri, P.; Pohl, K.; Wieghardt, K.; Nuber, B.; Weiss, J.; Papaefthymiou, G. C.; Frankel, R. B.; Lippard, S. J. *J. Am. Chem. Soc.* **1987**, *109*, 7387–7396.
(28) Davey, D. D. *J. Org. Chem.* **1987**, *52*, 4379–4381.
(29) Hoffmann, P.; Steinhoff, A.; Mattes, R. *Z. Naturforsch., B: Chem. Sci.* **1987**, *42b*, 867–873.
(30) Gahan, L.; Lawrance, G.; Sargeson, A. *Aust. J. Chem.* **1982**, *35*, 1119–1131.
(31) Boeyens, J. C. A.; Dobson, S. M.; Hancock, R. D. *Inorg. Chem.* **1985**, *24*, 3073–3076.

[LFeCl$_2$]PF$_6$. To a solution of 0.40 g (0.71 mmol) of [LFeCl$_2$]-FeCl$_4$ in 50 mL of dry methanol was added via cannula a solution of 0.14 g (0.85 mmol) of $NaPF_6$ in 30 mL of methanol. After the mixture was stirred for 1 h, an orange precipitate formed. The reaction mixture was further concentrated, and the solid was isolated by filtration and dried under vacuum. Yield: 0.36 g (0.70 mmol, 99%). X-ray quality crystals were obtained by vapor diffusion of diethyl ether into an acetonitrile solution of [LFeCl$_2$]PF$_6$ at room temperature. Electronic absorption (acetonitrile) λ_{max} (ε_M): 213 (1086), 309 (684), 426 (sh) (182). IR (KBr pellet), cm^{-1}: 3446 (br), 3292 (s), 3158 (m), 3131 (m), 1500 (m), 1480 (w), 1457 (m), 1423 (w), 1167 (m), 1076 (m), 988 (m), 836 (vs), 762 (m), 681 (w), 558 (s). (+)ESI-MS, *m*/*z* calcd. for $[C_{11}H_{20}N_4SFeCl_2]^+$, $[LFeCl(OCH_3)]^+$ 362.06; Found, 362.07; $[L^{-H}FeCl]^+$ 330.04; Found, 330.04. Elem. anal. Calcd. for $C_{11}H_{20}N_4SFeCl_2PF_6$: C, 25.80; H, 3.94; N, 10.94. Found: C, 25.80; H, 4.01; N, 10.79.

[(LFeCl)$_2$O][PF$_6$]$_2$. To a solution of 0.14 g (0.26 mmol) of [LFeCl$_2$]PF$_6$ in 16 mL of acetonitrile at 0 °C was added a solution of 75 μL (0.52 mmol) of triethylamine in 2 mL of acetonitrile. After the mixture was stirred for 2 h at room temperature, a solution of $NaPF_6$ 0.022 g (0.13 mmol) in 4 mL of methanol was added, and the mixture was stirred for an additional 2 h. The solvent was evaporated to obtain a brown oily compound which was washed with methanol and dried under vacuum. Single crystals were obtained by vapor diffusion of ether into acetone solutions of **3**. Yield: 0.12 g (0.12 mmol, 95%). IR (KBr pellet), cm^{-1}: 3428 (br), 3078 (m), 2882 (m), 1504 (m), 1400 (m), 1102 (m), 1076 (m), 839 (vs), 816 (s), 790 (m), 559 (s). (+)ESI-MS, *m*/*z* calcd. for $[C_{22}H_{40}N_8S_2Fe_2Cl_2O]^+$, $[(LFeCl)_2O]^{2+}/2]$ 339.04; Found, 339.05. Elem. anal. Calcd. for $C_{22}H_{40}N_8S_2Fe_2Cl_2OP_2F_{12}$: C, 27.26; H, 4.16; N, 11.56. Found: C, 27.72; H, 4.54; N, 11.39.

If addition of $NaPF_6$ is omitted during the synthesis, a crude product containing a mixture of [(LFeCl)$_2$O][PF$_6$]$_2$ and [(LFeCl)$_2$O][PF$_6$]Cl is obtained. The products can be separated by vapor diffusion of diethyl ether into an acetone solution of the crude product as yellow-orange prism shaped crystals of [(LFeCl)$_2$O][PF$_6$]$_2$ and red-orange block shaped crystals of [(LFeCl)$_2$O][PF$_6$]Cl. Crystals of [(FeCl)$_2$O][PF$_6$]Cl were of suitable quality for X-ray diffraction studies, while repeated crystallization attempts consistently yielded [(LFeCl)$_2$O]-[PF$_6$]$_2$ crystals of insufficient quality for X-ray analysis.

Catalytic Trials. A 0.36 mM solution of 4-nitrophenyl acetate was prepared in 3:1 mixture of NaH_2PO_4/Na_2HPO_4 buffer (pH = 6.00) and methanol. Duplicate samples were prepared by adding 0.2 equiv of [LFeCl$_2$]PF$_6$ to 10 mL aliquots of the 4-nitrophenyl acetate solution. An additional 10 mL aliquot of the 4-nitrophenyl acetate solution was taken as reference. The UV−visible spectrum was recorded for each aliquot over a period of 74 h. Comparison to a reference sample revealed no catalytic hydrolysis activity. Attempts with a pH = 3.8 NaH_2PO_4/Na_2HPO_4 buffer yielded similar results.

Physical Methods. Elemental analyses were obtained from Midwest Microlab (Indianapolis, IN). Infrared spectra were recorded with a Thermo Nicolet Avatar 360 spectrometer at 4 cm^{-1} resolution. NMR spectra were obtained with a Varian Inova500 500 MHz spectrometer. Electrospray ionization mass spectrometry (ESI-MS) was performed by the Laboratory for Biological Mass Spectrometry at Texas A&M University. Electronic absorption spectra were recorded with an Agilent 8453 diode array spectrometer with 1 cm path length quartz cells. The pK_a values for $[LFeCl-OH_2]^{2+}$ were determined spectrophotometrically in aqueous phosphate buffer using a Corning pH 440 m with full details in the Supporting Information. X-band electron paramagnetic resonance (EPR) spectra were obtained with a Bruker EMX EPR spectrometer at 77 K in a Suprasil quartz Dewar flask.

Crystallographic Studies. An orange block 0.34 × 0.16 × 0.06 mm^3 crystal of [LFeCl$_2$]FeCl$_4$ was mounted on a glass fiber for collection of X-ray data on a Bruker SMART APEX CCD diffractometer. The SMART[32] software package (v 5.632) was used to acquire a total of 1,868 thirty-second frame ω-scan exposures of data at 100 K to a $2\theta_{max}$ = 56.50° using monochromated Mo Kα radiation (0.71073 Å) from a sealed tube and a monocapillary. Frame data were processed using SAINT[33] (v 6.45) to determine final unit cell parameters: a = 13.0605(6)Å, b = 10.4331(5) Å, c = 16.1935(7) Å, β = 110.2420(10)°, V = 2070.27(16) Å^3, D_{calc} = 1.812 Mg/m3, Z = 4 to produce raw *hkl* data that were then corrected for absorption (transmission max./min. = 0.915/0.646; μ = 1.812 mm^{-1}) using SADABS[34] (v 2.10). The structure was solved by Patterson methods in the space group $P2_1/c$ using SHELXS-90[35] and refined by least-squares methods on F^2 using SHELXL-97[36] incorporated into the SHELXTL[37] (v 6.14) suite of programs. All non-hydrogen atoms were refined with anisotropic atomic displacement parameters. The amine hydrogen atom was located by difference maps and refined isotropically. Remaining hydrogen atoms were placed in their geometrically generated positions and refined as a riding model. Methylene and Im H atoms were included as fixed contributions with U(H) = 1.2 × U_{eq} (attached C atom) while methyl groups were allowed to ride (the torsion angle which defines its orientation was allowed to refine) on the attached C atom, and these atoms were assigned U(H) = 1.5 × U_{eq}. For all 4911 unique reflections (R(int) 0.025) the final anisotropic full matrix least-squares refinement on F^2 for 223 variables converged at R1 = 0.035 and wR2 = 0.067 with a GOF of 1.04.

X-ray structural analysis for [LFeCl$_2$]PF$_6$ was performed on a 0.16 × 0.14 × 0.07 mm^3 yellow-orange prism using an identical data acquisition strategy described above for [LFeCl$_2$]FeCl$_4$ at 100 K to a $2\theta_{max}$ = 55.20°. [LFeCl$_2$]PF$_6$ crystallizes in the space group $P2_1/c$ with unit cell parameters a = 7.6275(8) Å, b = 14.4722(15) Å, c = 16.9469(17) Å, β = 93.766(2)°, V = 1866.7(3) Å^3, Z = 4, and D_{calc} = 1.822 Mg/m^3. A total of 4277 raw independent data were corrected for absorption (transmission max./min. = 0.911/0.813; μ = 1.353 mm^{-1}) using SADABS. The structure was solved by Patterson methods using SHELXTL.[37] The hexafluorophosphate anion was modeled with a spinning-top disorder using one four-atom group of 70% occupancy (F3a−F6a) and a second four-atom group of 30% occupancy (F3b−F6b) in addition to the two full occupancy F atoms (F1 and F2). Fluorines 3b-6b were refined isotropically while all other non-hydrogen atoms were refined with anisotropic atomic displacement parameters. The amine hydrogen atom was located by difference maps and refined isotropically. Methyl, methylene, and Im H atoms were included as fixed contributions as described above for [LFeCl$_2$]FeCl$_4$. For all 4277 unique reflections (R(int) 0.034) the final anisotropic full matrix least-squares refinement on F^2 for 240 variables converged at R1 = 0.065 and wR2 = 0.116 with a GOF of 1.08.

An red-orange "cube" 0.23 × 0.22 × 0.21 mm^3 crystal of [(LFeCl$_2$)O][PF$_6$]Cl was mounted on a glass fiber for collection of X-ray data on a Bruker SMART APEX CCD diffractometer using an identical data acquisition strategy described above for [LFeCl$_2$]FeCl$_4$ at 100 K to a $2\theta_{max}$ = 50.12°. Frame data were processed using SAINT[33] (v 6.45) to determine final unit cell parameters a = 8.7061(4) Å, b = 16.0693(8) Å, c = 23.5679(12) Å, $\alpha = \beta = \gamma$ = 90°, V = 3297.2(3) Å^3, D_{calc} = 1.732 Mg/m^3,

(32) *SMART* (v.5632); Bruker Advanced X-ray Solutions, Inc.: Madison, WI, 2005.
(33) *SAINT* (v6.45a); Bruker Advanced X-ray Solutions, Inc.: Madison, WI, 2003.
(34) *SADABS, Area Detector Absorption Correction* (v2.10); University Göttingen: Göttingen, Germany, 2003.
(35) Sheldrick, G. M. *Acta Crystallogr.* **1990**, *A46*, 467.
(36) *SHELXL-97, Program for the Refinement of Crystal Structures*; University Göttingen: Göttingen, Germany, 1997.
(37) *SHELXTL, Program Library for Structure Solution and Molecular Graphics* (v6.14); Bruker Advanced X-ray Solutions, Inc.: Madison, WI, 2000.

$Z = 4$ to produce raw *hkl* data that were then corrected for absorption (transmission max./min. = 0.781/0.735; μ = 1.367 mm^{-1}) using SADABS[34] (v 2.10). The structure was solved by Patterson methods using SHELXTL.[37] All non-hydrogen atoms were refined with anisotropic atomic displacement parameters. The amine hydrogen atoms were located by difference maps and refined isotropically. Methyl, methylene, and Im H atoms were included as fixed contributions as described above for $[LFeCl_2]FeCl_4$. For all 6140 unique reflections (R(int) 0.031) the final anisotropic full matrix least-squares refinement on F^2 for 404 variables converged at R1 = 0.032 and wR2 = 0.077 with a GOF of 1.09. The absolute structure was determined by refinement of the Flack parameter (0.021(13)).

Electrochemical Studies. Cyclic voltammetry (CV) was performed using a PAR 273 potentiostat with a three electrode cell (glassy carbon working electrode, platinum wire counter electrode, and Ag wire pseudo reference electrode) at room temperature. For non-aqueous solutions, 0.1 M tetrabutylammonium hexafluorphosphate (TBAHFP) was employed as supporting electrolyte. In aqueous solutions, buffer (0.5 M) served as the supporting electrolyte. All potentials were scaled to a ferrocene/ferrocenium standard using an internal reference. Cyclic voltammetry (CV) experiments were conducted at room temperature with an analyte concentration of 1.0 mM. A background voltammogram was collected and subtracted from the measured sample data prior to analysis. For each set of data, the CV was fit using the DigiSim software package.[38] The diffusion coefficient was treated as a variable parameter with an initial setting of 10^{-6} cm^2/s. The standard rate constant (k_s) was set to 2×10^{-3} and 2×10^{-4} cm/s in methanol and aqueous buffer solutions, respectively, with a transfer coefficient, α, of 0.4. The standard half potentials E_1 and E_2 were estimated based on the potentials of minimum and maximum current and allowed to refine freely. The equilibrium constant K_1 was treated as a variable parameter in methanol, but set to the measured K_a value for $[(LFeCl)_2OH]^{3+}$ in aqueous buffer. K_2 was calculated from K_1 and the standard half potentials.

Results and Discussion

Synthesis and Characterization. The synthetic pathways to the tetradentate ligand 4-((1-methyl-1*H*-imidazol-2-yl)methyl)-1-thia-4,7-diazacyclononane (L) and its iron(III) derivatives are shown in Scheme 1. The ligand is prepared by reductive amination following previously developed strategies for the attachment of pendant imidazole donors to amines.[39−43] Addition of 1.4 equiv of 1-methyl-1*H*-imidazole-2-carboxaldehyde to 1-thia-4,7-diazacylcononane (TASN) yields L upon sodium borohydride reduction in 78% yield following column purification. Addition of L to $FeCl_3$ (2 equiv) in methanol yields $[LFeCl_2]FeCl_4$ as a dark red precipitate. Exchange of $FeCl_4^-$ by PF_6^- yields $[LFeCl_2]PF_6$ in which the cation has isomerized to an alternate diastereomer. The three nitrogen donors of L are in a facial arrangement in the $FeCl_4^-$ salt and a meridional orientation in the PF_6^- salt (vide infra). The isomerization is attributed to the lability of one of the chloride donors in protic solvents. Dissociation of a single chloride in methanol is supported by the positive ion mode electrospray mass spectrum ((+)ESI-MS) of $[LFeCl_2]FeCl_4$. Isotopic envelopes with m/z values consistent with $[LFeCl_2]^+$ (366.00), $[LFeCl(OCH_3)]^+$ (362.06), $[LFeCl(OH)]^+$ (348.03), and $[L^{-H}FeCl]^+$ (330.06) are observed, Supporting Information, Figure S1. The (+)ESI-MS of $[LFeCl_2]PF_6$ in methanol yields similar results, Supporting Information, Figure S2.

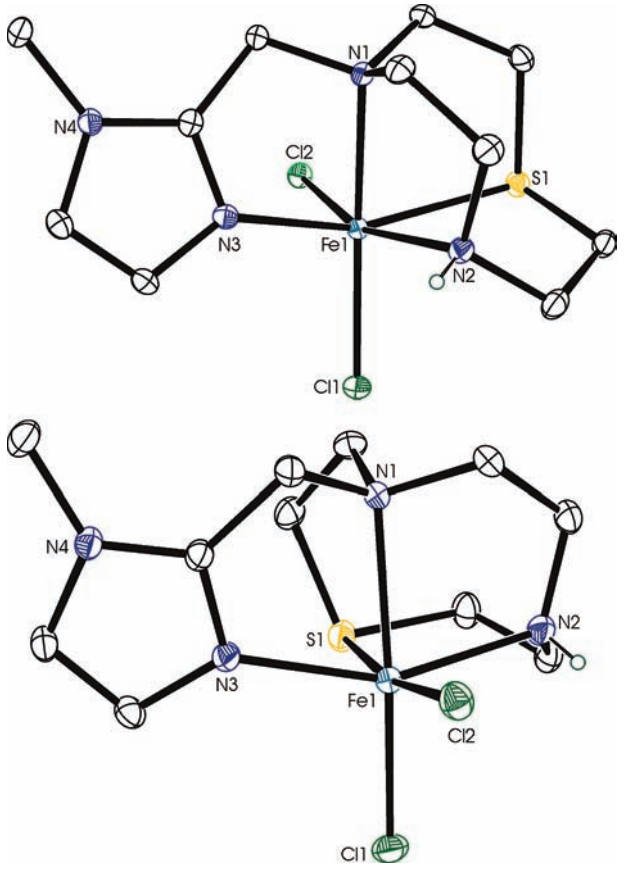

Figure 1. ORTEP representation of the cation portions of $[LFeCl_2]FeCl_4$ (top) and $[LFeCl_2]PF_6$ (bottom) illustrating the facial and meridional coordination of the three nitrogen donors of the tetradentate ligand L, respectively. Selected bond distances and angles provided in Table 2.

The X-band EPR of $[LFeCl_2]PF_6$ in frozen methanol at 77 K displays a single resonance at $g = 4.3$ consistent with a $S = 5/2$ high-spin Fe(III) ion in a rhombic environment. The UV−visible spectrum of $[LFeCl_2]PF_6$ in acetonitrile reveals a broad charge transfer band at 309 nm (ε = 6830 M^{-1} cm^{-1}) with a shoulder at 426 nm. The addition of base shifts the absorbance maximum to 300 nm (ε = 15,300 M^{-1} cm^{-1}) with shoulders at 332 and 382 nm because of the formation of the μ-oxo complex $[(LFeCl)_2O]^{2+}$. The ESI-MS of $[(LFeCl)_2O]^{2+}$ in methanol displays an isotopic envelope at m/z = 339.05 ($z = 2$) as expected for the dicationic complex, $[(LFeCl)_2O]^{2+}$. The ESI-MS shows no evidence of chloride dissociation from the μ-oxo diiron core. The infrared spectrum of $[(LFeCl)_2O][PF_6]_2$ displays a new band at 816 cm^{-1} assigned to the Fe−O−Fe asymmetric stretch.

X-ray Crystal Structure Analysis. The structures of $[LFeCl_2]FeCl_4$, $[LFeCl_2]PF_6$, and $[(LFeCl)_2O][PF_6]Cl$ were determined by single crystal X-ray diffraction techniques. Oak Ridge Thermal-Ellipsoid Plot (ORTEP) representations

(38) *DigiSim*; Bioanalytical Systems, Inc.: West Lafayette, IN, 2004.
(39) Cheruzel, L. E.; Wang, J. P.; Mashuta, M. S.; Buchanan, R. M. *Chem. Commun.* **2002**, 2166–2167.
(40) Chen, S.; Richardson, J. F.; Buchanan, R. M. *Inorg. Chem.* **1994**, *33*, 2376–2382.
(41) Oberhausen, K. J.; O'Brien, R. J.; Richardson, J. F.; Buchanan, R. M. *Inorg. Chim. Acta* **1990**, *173*, 145–154.
(42) Oberhausen, K. J.; Richardson, J. F.; Buchanan, R. M.; Pierce, W. *Polyhedron* **1989**, *8*, 659–668.
(43) Cheruzel, L. E.; Cecil, M. R.; Edison, S. E.; Mashuta, M. S.; Baldwin, M. J.; Buchanan, R. M. *Inorg. Chem.* **2006**, *45*, 3191–3202.

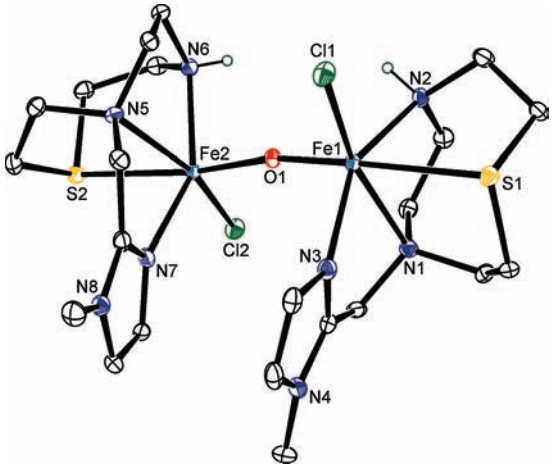

Figure 2. ORTEP representation of the cation $[(LFeCl)_2O]^{2+}$. Selected bond distances and angles provided in Table 2.

of the cationic complexes are shown in Figures 1 and 2. Crystallization of $[(LFeCl)_2O][PF_6]_2$ consistently yielded poor diffraction quality yellow-orange crystals unsuitable for X-ray analysis. Details of the data collection and refinement are summarized in Table 1. Selected bond distances and angles are provided in Table 2.

Orange block shaped crystals of $[LFeCl_2]FeCl_4$ in the monoclinic space group $P2_1/c$ were obtained by slow evaporation of dichloromethane solutions. As shown in Figure 1 (top), iron is coordinated in a pseudo-octahedral N_3SCl_2 donor environment. The N_2S donors of the TASN ring define one face of the octahedron. The pendant imidazole nitrogen (N3) sits trans to the thioether donor S1 with an N3−Fe−S1 bond angle of 159.01(5)° resulting in facial coordination of the three N donors. The two chloride donors Cl1 and Cl2 occupy cis positions with a Cl1−Fe−Cl2 bond angle of 99.86(2)°. The bond distances to the TASN backbone of 2.2291(16), 2.1951(18), and 2.5320(6) Å for the Fe−N1, Fe−N2, and Fe−S1 bonds are consistent with high-spin iron(III).[44,45] The Fe−N3 bond distance of 2.0479(17) Å is similar to Fe−N_{imid} distances in related complexes. The Fe−Cl bond distances are 2.2617(6) and 2.2967(5) Å for Cl1 and Cl2, respectively.

Anion exchange of PF_6^- for $FeCl_4^-$ yields yellow-orange prism shaped crystals of $[LFeCl_2]PF_6$ also in the $P2_1/c$ space group. As shown in Figure 1 (bottom), the complex cation is a diasteromer of $FeCl_4^-$ derivative. In the PF_6^- salt, the imidazole nitrogen (N3) is trans to the secondary amine N2 with a N2−Fe−N3 bond angle of 154.33(13)°. The three N donors are arranged in a meridional orientation as opposed to the facial coordination of $[LFeCl_2]FeCl_4$. The bond distances to the TASN N_2S core are slightly longer in the PF_6^- derivative with values of 2.291(3), 2.139(3), and 2.5735(12) Å, respectively for N1, N2, and S1. The Fe−N3 bond distance of 2.056(3) Å is within experimental error of the $FeCl_4^-$ derivative. Neither structure shows evidence of obvious packing forces such as H-bonding or π-interactions that would favor one diastereomer over the other.

The isomerization of the $[LFeCl_2]^+$ core is proposed to involve dissociation of Cl2 during the anion exchange reaction in methanol. In both isomers, the chloride donors can be distinguished based on Fe−Cl bond distances. The immobile chloride, Cl1, sits trans to the tertiary amine, N1, while the labile chloride, Cl2, occupies a position trans to the secondary amine, N2, in the $FeCl_4^-$ salt and the thioether sulfur, S1, in the PF_6^- salt. In the former, the Fe−Cl2 bond distance is 0.0350(8) Å longer than Fe−Cl1 consistent with its selective dissociation. The Fe−Cl2 bond distance decreases slightly, 0.009(1) Å, as compared to the other isomer of $[LFeCl_2]^+$, while the Fe−Cl1 bond gets significantly shorter, 0.032(1) Å. These results support our hypothesis that Cl2 remains labile, while the Fe−Cl bond to the immobile Cl1 is further stabilized.

The μ-oxo complex $[(LFeCl)_2O][PF_6]Cl$ crystallizes as red-orange blocks in the orthorhombic space group $P2_12_12_1$. The dicationic complex $[(LFeCl)_2O]^{2+}$, Figure 2, contains two independent iron(III) ions with similar N_3SClO pseudo-octahedral environments. The three N donors of L are oriented in a meridional fashion as observed in the $[LFeCl_2]PF_6$ precursor. The oxo atom O1 sits in the position trans to S1 that was formerly occupied by the labile chloride, Cl2. The Fe−N distances to the TASN backbone of 2.298(3) and 2.152(3) Å for Fe1−N1 and Fe1−N2 are within experimental uncertainty of the values in $[LFeCl_2]PF_6$. The Fe1−N3 and Fe2−N7 bond distances to the coordinated imidazole of 2.113(3) and 2.086(3) Å are slightly longer than in the dichloro precursor. The iron-oxo bond distances of 1.791(2) and 1.803(2) Å for Fe1−O1 and Fe2−O1 are typical of Fe−O−Fe complexes. The Fe1−O1−Fe2 bond angle is 168.47(13)°. The trans influence of the iron-oxo bonds results in a substantial increase in the iron−sulfur bond distances with values of 2.6535(9) and 2.6491(9) Å for Fe1−S1 and Fe2−S2.

The Fe−O−Fe core of $[(LFeCl)_2O]^{2+}$ is supported by non-covalent interactions including π-stacking and H-bonding, Supporting Information, Figure S4. The N3 and N7 containing imidazole rings are oriented in a face to face π-stacking interaction. The centroid to centroid distance between the N3 and N7 rings is 3.4270(19) Å with a plane−plane angle of 7.97°. These values fall in a typical range for π-stacking interactions of nitrogen containing ligands. The secondary amines N2 and N6 trans to the imidazole rings support the oxo-bridge through H-bonding interactions with a symmetry chloride counterion Cl3′ $(1 - x, 1/2 + y, 1/2 - z)$. The donor−acceptor distance is 3.205(3) Å for the N2···Cl3′ interaction, while the N6···Cl3′ donor−acceptor distance is slightly shorter at 3.145(3) Å. Using the located positions of the H-atoms, the H2n···Cl3′ and H6n···Cl3′ distances are 2.29(4) and 2.41(3) Å with N2−H2n−Cl3′ and N6−H6n−Cl3′ angles of 162(3) and 154(3)°. The H-acceptor distances are near the average value of 2.27 reported by Brammer for N−H···Cl hydrogen bonds.[46]

Aqueous Studies. As noted above, one chloride readily dissociates from $[LFeCl_2]^+$ in methanol leading to isomerization of the solid state structure and methoxide/hydroxide coordination in gas phase based on mass

(44) Grillo, V. A.; Hanson, G. R.; Hambley, T. W.; Gahan, L. R.; Murray, K. S.; Moubaraki, B. *J. Chem. Soc., Dalton Trans.* **1997**, 305–312.
(45) Grillo, V. A.; Gahan, L. R.; Hanson, G. R.; Stranger, R.; Hambley, T. W.; Murray, K. S.; Moubaraki, B.; Cashion, J. D. *J. Chem. Soc., Dalton Trans.* **1998**, *0*, 2341–2348.
(46) Brammer, L.; Bruton, E. A.; Sherwood, P. *Cryst. Growth Des.* **2001**, *1*, 277–290.

Table 1. Crystal Data and Structure Refinement for $[LFeCl_2]FeCl_4$, $[LFeCl_2]PF_6$, and $[(LFeCl)_2O]ClPF_6$

identification code	$[LFeCl_2]FeCl_4$	$[LFeCl_2]PF_6$	$[(LFeCl)_2O]ClPF_6$
empirical formula	$C_{11}H_{20}Cl_2FeN_4S \cdot FeCl_4$	$C_{11}H_{20}Cl_2FeN_4SPF_6$	$C_{22}H_{40}Cl_2Fe_2N_8OS_2 \cdot Cl \cdot PF_6$
formula weight	564.77	512.09	859.76
temperature (K)	100(2)	100(2)	100(2)
wavelength (Å)	0.71073	0.71073	0.71073
crystal system	monoclinic	monoclinic	orthorhombic
space group	$P2_1/c$	$P2_1/c$	$P2_12_12_1$
unit cell dimensions			
a (Å)	13.0605(6)	7.6275(8)	8.7061(4)
b (Å)	10.4331(5)	14.4722(15)	16.0693(8)
c (Å)	16.1935(7)	16.9469(17)	23.5679(12)
β (deg)	110.2420(10)	93.766(2)	90
volume (Å^3)	2070.27(16)	1866.7(3)	3297.2(3)
Z	4	4	4
density (Mg/m^3) (calculated)	1.812	1.822	1.732
absorption coefficient (mm^{-1})	2.279	1.353	1.367
$F(000)$	1136	1036	1760
crystal size (mm^3)	$0.34 \times 0.16 \times 0.06$	$0.16 \times 0.14 \times 0.07$	$0.24 \times 0.22 \times 0.19$
θ range for data collection (deg)	1.66−28.25	1.85−27.60	2.49 − 25.56
index ranges	$-17 \le h \le 17$	$-9 \le h \le 9$	$-10 \le h \le 10$
	$-13 \le k \le 13$	$-18 \le k \le 18$	$-19 \le k \le 19$
	$-21 \le l \le 21$	$-22 \le l \le 22$	$-27 \le l \le 28$
reflections collected	18134	16212	25598
independent reflections	4911 [R(int) = 0.0252]	4277 [R(int) = 0.0344]	6140 [R(int) = 0.0307]
completeness to	θ = 28.25°	θ = 27.60°	θ = 25.56°
	95.8%	98.9%	99.7%
absorption correction	SADABS	SADABS	SADABS
max. and min transmission	0.915 and 0.6726	0.911 and 0.813	0.781 and 0.735
refinement method	full-matrix least-squares on F^2	full-matrix least-squares on F^2	full-matrix least-squares on F^2
data/restraints/parameters	4911/0/223	4277/3/240	6140/0/404
goodness-of-fit on F^2	1.042	1.079	1.091
final R indices [$I > 2\sigma(I)$]	R1 = 0.0284	R1 = 0.0567	R1 = 0.0312
	wR2 = 0.0643	wR2 = 0.1124	wR2 = 0.0764
R indices (all data)	R1 = 0.0348	R1 = 0.0650	R1 = 0.0324
	wR2 = 0.0672	wR2 = 0.1164	wR2 = 0.0772
largest diff. peak and hole (e Å^{-3})	0.683 and −0.358	1.306 and −0.672	0.899 and −0.651

spectrometry. Further, $[LFeCl_2]^+$ cleanly converts to the μ-oxo derivative $[(LFeCl)_2O]^{2+}$ upon the addition of base in acetonitrile. Therefore, we decided to investigate the aqueous chemistry of $[LFeCl_2]^+$ as a function of pH. All studies were conducted on freshly prepared solutions because of complex degradation over a period of several hours in water.

Aqueous solutions (NaH_2PO_4/Na_2HPO_4 buffer) of $[LFeCl_2]PF_6$ yield three accessible species as a function of pH, Scheme 2. We assign the spectrum observed under mildly acidic conditions (pH = 5) with an absorbance maximum at 282 nm (ε = 4900 M^{-1} cm^{-1}) to the μ-OH hydroxide complex $[(LFeCl)_2(OH)]^{3+}$. The bridging hydroxide can be protonated or deprotonated by modulating the pH. An alternate assignment for the amphoteric complex based on a recent report by Chavez and coworkers is $[L(H_2O)Fe(\mu\text{-}O)Fe(OH)L]$.[8] This is disfavored as H-bonding between the H_2O and HO^- would be expected to bend the Fe−O−Fe bond.[47] Bent μ-oxo diiron complexes typically display an oxo to iron(III) charge transfer band near 480 nm that is forbidden in linear complexes.[48]

Titration of pH = 5 buffered solutions of $[(LFeCl)_2(OH)]^{3+}$ with NaOH yields the μ-oxo diiron complex $[(LFeCl)_2(O)]^{2+}$ as indicated by the decrease in band intensity at 284 nm and an increase at 214 nm, Figure 3. Isosbestic points are observed at 236 and 334 nm. Titration of the $[(LFeCl)_2(OH)]^{3+}$ solution with H_3PO_4 yields the aqua derivative $[LFeCl(OH_2)]^{2+}$ with intensity decrease at 282 nm and isosbestic points at 238 and 413 nm, Supporting Information, Figure S5. From this data, pK_a values 3.8 ± 0.1 and 6.1 ± 0.3 were calculated for $[LFeCl(OH_2)]^{2+}$ and $[(LFeCl)_2(OH)]^{3+}$, respectively. Previously, we reported the stepwise titration $[(bmmp\text{-}TASN)Fe{-}OH_2]^+$ (bmmp-TASN = *N*,*N*′-4,7-bis-(2′-methyl-2′-mercaptopropyl)-1-thia-4,7-diazacyclononane) in methanol/water to the μ-OH and μ-O complexes $[((bmmp\text{-}TASN)Fe)_2OH]^+$ and $((bmmp\text{-}TASN)Fe)_2O$, respectively, with measured pK_a values 5.4(1) and 6.52(5).[49] The structures of the diiron complexes were confirmed by X-ray crystallography. The complexes in the current study are more acidic consistent with their higher positive charge, and the proposed unsupported oxo- and hydroxo-bridges, Scheme 2, do not display weak charge transfer transitions usually observed for supported Fe(III)−O(H)−Fe(III) species.[6]

On the basis of the pK_a measurements, aqueous solutions of $[LFeCl_2]PF_6$ should consist primarily of the hydroxide bound derivative $[(LFeCl)_2(OH)]^{3+}$ under mildly acidic conditions. Attempts to hydrolyze 4-nitrophenyl acetate in NaH_2PO_4/Na_2HPO_4 buffer were followed by UV−visible spectroscopy at pH = 6.00 and 3.80. Trials in the presence and absence of $[LFeCl_2]PF_6$ were indistinguishable. The lack of hydrolytic activity is

(47) Hazell, A.; Jensen, K. B.; McKenzie, C. J.; Toftlund, H. *Inorg. Chem.* **1994**, *33*, 3127–3134.
(48) Brown, C. A.; Remar, G. J.; Musselman, R. L.; Solomon, E. I. *Inorg. Chem.* **1995**, *34*, 688–717.
(49) O′Toole, M. G.; Bennett, B.; Mashuta, M. S.; Grapperhaus, C. A. *Inorg. Chem.* **2009**, *48*, 2300–2308.

Table 2. Selected Bond Distances (Å) and Bond Angles (deg) for $[LFeCl_2]FeCl_4$, $[LFeCl_2]PF_6$, and $[(LFeCl)_2O]ClPF_6$[a]

	$[LFeCl_2]FeCl_4$	$[LFeCl_2]PF_6$	$[(LFeCl)_2O]ClPF6$
$Fe-N_{am2°}$	2.1951(18)	2.139(3)	2.152(3)
			2.141(3)
$Fe-N_{am3°}$	2.2291(16)	2.291(3)	2.298(3)
			2.305(3)
$Fe-N_{imid}$	2.0479(17)	2.056(3)	2.113(3)
			2.086(3)
Fe−S	2.5320(6)	2.5735(12)	2.6535(9)
			2.6491(9)
$Fe-Cl_a$	2.2617(6)	2.2299(11)	2.3138(9)
			2.2773(8)
$Fe-Cl_b$	2.2967(5)	2.2874(11)	
Fe−O			1.791(2)
			1.803(2)
$N_{am3°}-Fe-N_{am2°}$	79.21(6)	77.50(12)	77.47(10)
			77.51(10)
$N_{am3°}-Fe-N_{imid}$	76.39(6)	77.66(12)	75.10(10)
			75.37(10)
$N_{am2°}-Fe-N_{imid}$	96.88(7)	154.33(13)	150.38(10)
			150.50(11)
$N_{am3°}-Fe-S$	82.69(4)	79.48(9)	78.94(7)
			78.89(7)
$N_{am2°}-Fe-S$	77.18(5)	81.43(10)	79.12(8)
			79.25(8)
$N_{imid}-Fe-S$	159.01(5)	87.78(10)	84.84(7)
			84.32(7)
$N_{am3°}-Fe-Cl_a$	169.45(5)	165.94(9)	163.63(7)
			162.93(7)
$N_{am2°}-Fe-Cl_a$	91.65(5)	100.33(10)	101.08(8)
			101.57(8)
$N_{imid}-Fe-Cl_a$	99.75(5)	102.18(9)	102.06(8)
			100.94(8)
$S-Fe-Cl_a$	100.53(2)	86.46(4)	84.76(3)
			84.18(3)
$N_{am3°}-Fe-Cl_b$	90.34(4)	93.77(9)	
$N_{am2°}-Fe-Cl_b$	161.31(5)	91.37(10)	
$N_{imid}-Fe-Cl_b$	95.64(5)	96.61(10)	
$Cl_a-Fe-Cl_b$	99.86(2)	100.19(4)	
$S-Fe-Cl_b$	86.210(19)	171.02(4)	
Fe−O−Fe			168.47(13)

[a] $N_{am2°}$ = secondary amine (N2, N6); $N_{am3°}$ = tertiary amine (N1, N5); N_{imid} = imidazole nitrogen (N3, N7); Cl_a = chloride trans $N_{am3°}$; Cl_b = chloride trans to $N_{am2°}$ or S.

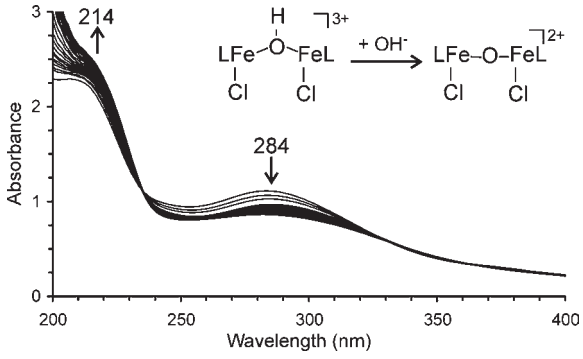

Figure 3. UV−visible trace recorded during the titration of $[(LFeCl)_2OH]^{3+}$ in 0.5 M NaH_2PO_4/Na_2HPO_4 buffer from pH = 4.64 to 7.87 with NaOH.

Scheme 2. Acid/Base Equilibria of $[LFeCl(OH_2)]^{2+}$

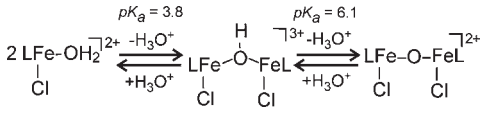

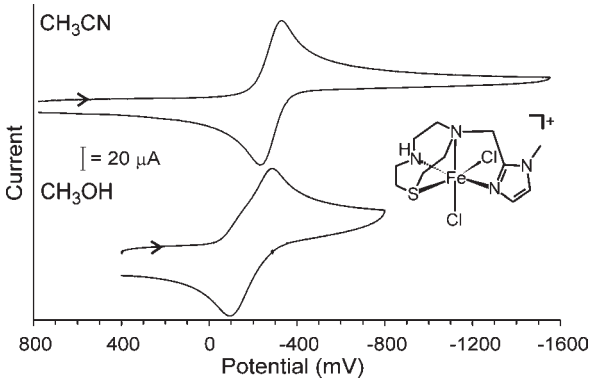

Figure 4. Cyclic voltammograms of $[LFeCl_2]PF_6$ in acetonitrile (top) and methanol (bottom) with 0.1 M TBAHFP supporting electrolyte. Scan rate = 200 mV/s. Potentials scaled to ferrocene.

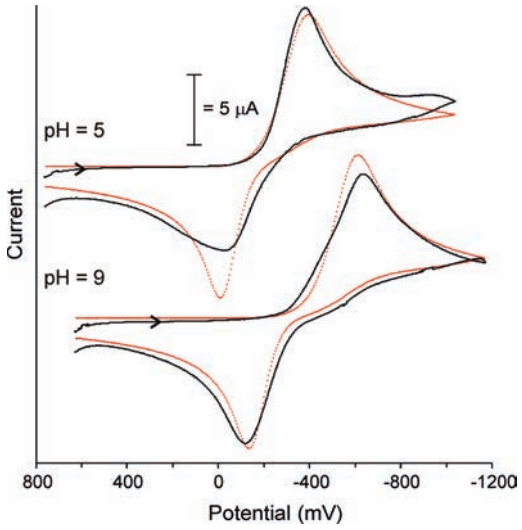

Figure 5. Experimental (solid black) and simulated (dotted red) cyclic voltammograms of $[LFeCl_2]PF_6$ in aqueous solution at pH = 5 (top) and pH = 9 (bottom) in 0.5 M NaH_2PO_4/Na_2HPO_4 buffer. Scan rate = 200 mV/s. Potentials scaled to ferrocene.

in contrast to species with μ-oxo complexes with terminal hydroxide donors such as $[tpa(OH)FeOFe(H_2O)tpa]^{3+}$, which readily hydrolyzes acetonitrile yielding the μ-acetamido-*N,O* derivative.[47]

Electrochemical Investigations. Cyclic voltammograms (CV) of $[LFeCl_2]PF_6$ were recorded under various conditions to further investigate the solution properties of $[LFeCl_2]PF_6$. Selected voltammograms are shown in Figures 4 and 5. The results are summarized in Table 3. In all experiments, a three electrode cell was employed with a glassy carbon working electrode, a platinum wire counter electrode, and a silver wire pseudo reference electrode. All potentials were scaled to ferrocene (Fc) using an internal reference.

In acetonitrile, the $[LFeCl_2]^+$ complex remains intact with no evidence of chloride lability. As such, a single redox event assigned as the $Fe^{III/II}$ redox couple is observed at −280 mV (vs Fc^+/Fc) with a ΔE of 100 mV, Figure 4 (top). In methanol, the labile chloride of $[LFeCl_2]^+$ is in rapid equilibrium (K_1) with methoxide as shown in Scheme 3 resulting in a broadening of the cathodic wave, Figure 4 (bottom). This equilibrium requires substitution of chloride by methanol followed by solvent deprotonation, which is dependent on the oxidation state of iron. Reduction of Fe(III) to Fe(II)

Table 3. Electrochemical Data from Cyclic Voltammetry in Acetonitrile, Methanol, and Aqueous Buffer[a]

redox couple	$E_{1/2}$ (ΔE_p); mV	solvent
$[LFeCl_2]^{+/0}$	−280 (96)	CH_3CN
$[LFeCl_2]^{+/0}$	−170[b]	CH_3OH
$[LFeCl(OCH_3)]^{+/0}$	−440[b]	CH_3OH
$[(LFeCl)_2(OH)]^{3+/2+}$	−170[b]	H_2O
$[(LFeCl)_2(O)]^{2+/+}$	−390[b]	H_2O

[a] All potentials are measured at a scan rate of 200 mV/s and scaled to ferrocene. Aqueous solutions were buffered to pH = 5, 7, or 9 using NaH_2PO_4/Na_2HPO_4 with a total concentration of 0.5 M. Non-aqueous solutions contained 0.1 M TBAHFP as supporting electrolyte. [b] $E_{1/2}$ values derived from DigiSim simulations.

Scheme 3. Redox Equilibria in Methanol Solution

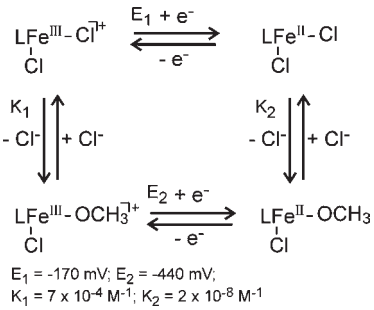

favors coordination of chloride over methoxide because of the decrease in Lewis acidity of iron. In the lower oxidation state, methanol is not effectively deprotonated and chloride coordination is preferred. As such, only a single anodic event is observed for the return wave. Simulations of the CV using the DigiSim software package[38] reveal $E_{1/2}$ values of −170 and −440 mV for the $[LFeCl_2]^{+/0}$ and $[LFeCl(OCH_3)]^{+/0}$ potentials, respectively. The potential for the $[LFeCl_2]^{+/0}$ couple is shifted by +110 mV compared to its value in acetonitrile attributable to H-bonding effects. From the digital simulations, the chloride dissociation constant for Fe(III), K_1, is estimated as 7×10^{-4} M^{-1}. From the redox potentials and K_1, the chloride dissociation constant for Fe(II), K_2, is calculated as 2×10^{-8} M^{-1}. As noted above, this four-order of magnitude shift in the chloride dissociation constant is attributed to the decreased acidity of methanol coordinated to Fe(II) as compared to Fe(III).

As described above, under mildly acidic conditions aqueous solutions of $[LFeCl_2]^+$ exists primarily as the hydroxide derivative $[(LFeCl)_2(OH)]^{3+}$. A series of CVs were recorded on freshly prepared aqueous solutions of $[LFeCl_2]^+$ to determine the effect of reduction on the pK_a of the bridging hydroxide and oxide derivatives. Figure 5 displays the experimental and simulated voltammograms at pH = 5 (top) and pH = 9 (bottom) at a scan rate of 200 mV. Scheme 4 summarizes the redox equilibria with full simulations details provided in the Experimental Section. At pH = 5.0, a 1 mM solution of $[LFeCl_2]^+$ is ∼90% the hydroxide derivative $[(LFeCl)_2(OH)]^{3+}$. The CV reveals a redox event (E_1) with an $E_{1/2}$ of −170 mV. The large peak separation was modeled using a small standard rate constant ($k_s = 2 \times 10^{-4}$ cm/s) that approaches the irreversible limit. An alternate model requiring high uncompensated resistance is rejected based on the high buffer concentration (0.5 M). A small degree of broadening results from contributions from the $[(LFeCl)_2(O)]^{2+/+}$ couple of −390 mV. The difference between the peak and half-peak potentials is consistent with a single electron transfer ($n = 1$) according to the formula $|E_{p/2} - E_p| = 47.7/\alpha n$ (mV, 25 °C) with an electron transfer coefficient (α) of 0.4.[50]

Scheme 4. Redox Equilibria in Aqueous Solution

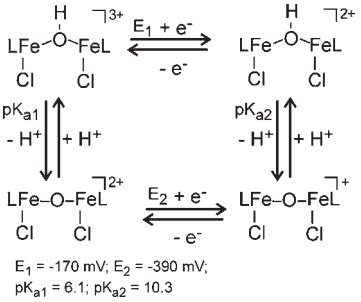

At pH = 9.0, the solution is primarily the μ-oxo derivative $[(LFeCl)_2(O)]^{2+}$. In acetonitrile, the reduction of $[(LFeCl)_2(O)]^{2+}$ is irreversible with an E_{pc} of −880 mV. In pH = 9 buffer, the redox potential (E_2) for the $[(LFeCl)_2(O)]^{2+/+}$ couple of −390 mV is shifted −220 mV with respect to the $[(LFeCl)_2(OH)]^{3+/2+}$ couple. As in the pH = 5 voltammogram, the current function suggests a single electron transfer based on the value $|E_{p/2} - E_p|$. The apparent peak separation ($\Delta E = 500$ mV) is too large to be attributed solely to slow electron transfer and reflects the equilibria outlined in Scheme 4. The value of pK_{a2} is calculated as 10.1 based on E_1, E_2, and pK_{a1} consistent with a marked decrease in the Lewis acidity of iron upon reduction. Reduction of $[(LFeCl)_2(O)]^{2+}$ to $[(LFeCl)_2(O)]^+$ at pH = 9 induces protonation to $[(LFeCl)_2(OH)]^{2+}$. The rapid protonation causes an anodic shift in the observed cathodic current maximum. Similarly, in the anodic direction the oxidation of $[(LFeCl)_2(OH)]^{2+}$ is facilitated by the rapid deprotonation of $[(LFeCl)_2(OH)]^{3+}$ resulting in an observed cathodic shift of the anodic current minimum. The mixed valent (Fe^{III}/Fe^{II}) derivative $[(LFeCl)_2(OH)]^{2+}$ degrades over several hours in aqueous solution, and efforts to isolate this complex were unsuccessful.

Conclusions

The non-heme iron complex $[LFeCl_2]^+$ was synthesized, and its solution properties explored in a variety of solvents including acetonitrile, methanol, and water. In acetonitrile, the complex remains coordinatively saturated as the nonprotic solvent is unable to effectively solvate the anionic chlorides. In methanol, a single chloride is partially dissociated yielding the methoxide derivative $[LFeCl(OCH_3)]^+$ in equilibrium with $[LFeCl_2]^+$. Reduction of the metal center from Fe(III) to Fe(II) disfavors deprotonation of coordinated methanol because of the lower Lewis acidity of Fe(II) as compared to Fe(III). This results in a 4 orders of magnitude shift in equilibrium toward the dichloro derivative. In water, a similar large shift in pK_a is observed. The aqua complex $[LFeCl(OH_2)]^{2+}$ displays two titration events with pK_a values of 3.8 ± 0.1 and 6.1 ± 0.3. The first deprotonation yields the hydroxide bridged complex $[(LFeCl)_2(OH)]^{2+}$. Structural characterization of unsupported hydroxide bridged complexes is rare.[20,49] This may be attributed in part to the small

(50) Bard, A. J.; Faulkner, L. R. *Electrochemical Methods Fundamentals and Applications*; John Wiley & Sons: New York, 1980.

pH window in which these complexes exist. Further deprotonation of $[(LFeCl)_2(OH)]^{3+}$ yields the μ-oxo derivative $[(LFeCl)_2(O)]^{2+}$. Reduction of $[(LFeCl)_2(OH)]^{3+}$ by one electron shifts the pK_a of the bridging hydroxide by four pH units to 10.3 similar to the results observed in methanol . As a result, reduction of the μ-oxo complex $[(LFeCl)_2(O)]^{2+}$ to the mixed valent species $[(LFeCl)_2(O)]^{+}$ favors protonation in all but strongly basic conditions.

Acknowledgment. Acknowledgment is made to the National Science Foundation (CHE-0749965) for funding. M.S.M. thanks the Department of Energy, Grant DE-FG02-08CH11538, and the Kentucky Research Challenge Trust Fund for upgrade of our X-ray facilities.

Supporting Information Available: (+)ESI-MS of $[LFeCl_2]FeCl_4$, $[LFeCl_2]PF_6$, and $[(LFeCl)_2O][PF_6]_2$, view of non-covalent interactions in the X-ray structure of $[(LFeCl)_2O][PF_6]Cl$, and UV−visible trace of the acidic titration of $[(LFeCl)_2OH]^{3+}$ in PDF format, and crystallographic data in CIF format (780376−780378). This material is available free of charge via the Internet at http://pubs.acs.org.